Prokineticin Receptor-1 Signaling Inhibits Dose- and Time-Dependent Anthracycline-Induced Cardiovascular Toxicity Via Myocardial and Vascular Protection

Adeline Gasser, Yue-Wen Chen, Anais Audebrand, Ayhan Daglayan, Marine Charavin, Brigitte Escoubet, Pavel Karpov, Igor V Tetko, Michael W.Y. Chan, Daniela Cardinale, et al.

JACC: CARDIOONCOLOGY VOL. 1, NO. 1, 2019

ORIGINAL RESEARCH

Prokineticin Receptor-1 Signaling Inhibits Dose- and Time-Dependent Anthracycline-Induced Cardiovascular Toxicity Via Myocardial and Vascular Protection

Adeline Gasser, PhD,[a] Yu-Wen Chen, MD, PhD,[b] Anais Audebrand, MSci,[a] Ayhan Daglayan, MSci,[a] Marine Charavin, PhD,[a] Brigitte Escoubet, MD, PhD,[c] Pavel Karpov, PhD,[d] Igor Tetko, PhD,[d] Michael W.Y. Chan, PhD,[e] Daniela Cardinale, MD,[f] Laurent Désaubry, PhD,[a] Canan G. Nebigil, PharmD, PhD[a]

ABSTRACT

OBJECTIVES This study investigated how different concentrations of doxorubicin (DOX) can affect the function of cardiac cells. This study also examined whether activation of prokineticin receptor (PKR)-1 by a nonpeptide agonist, IS20, prevents DOX-induced cardiovascular toxicity in mouse models.

BACKGROUND High prevalence of heart failure during and following cancer treatments remains a subject of intense research and therapeutic interest.

METHODS This study used cultured cardiomyocytes, endothelial cells (ECs), and epicardium-derived progenitor cells (EDPCs) for in vitro assays, tumor-bearing models, and acute and chronic toxicity mouse models for in vivo assays.

RESULTS Brief exposure to cardiomyocytes with high-dose DOX increased the accumulation of reactive oxygen species (ROS) by inhibiting a detoxification mechanism via stabilization of cytoplasmic nuclear factor, erythroid 2. Prolonged exposure to medium-dose DOX induced apoptosis in cardiomyocytes, ECs, and EDPCs. However, low-dose DOX promoted functional defects without inducing apoptosis in EDPCs and ECs. IS20 alleviated detrimental effects of DOX in cardiac cells by activating the serin threonin protein kinase B (Akt) or mitogen-activated protein kinase pathways. Genetic or pharmacological inactivation of PKR1 subdues these effects of IS20. In a chronic mouse model of DOX cardiotoxicity, IS20 normalized an elevated serum marker of cardiotoxicity and vascular and EDPC deficits, attenuated apoptosis and fibrosis, and improved the survival rate and cardiac function. IS20 did not interfere with the cytotoxicity or antitumor effects of DOX in breast cancer lines or in a mouse model of breast cancer, but it did attenuate the decreases in left ventricular diastolic volume induced by acute DOX treatment.

CONCLUSIONS This study identified the molecular and cellular signature of dose-dependent, DOX-mediated cardiotoxicity and provided evidence that PKR-1 is a promising target to combat cardiotoxicity of cancer treatments.
(J Am Coll Cardiol CardioOnc 2019;1:84–102) © 2019 The Authors. Published by Elsevier on behalf of the American College of Cardiology Foundation. This is an open access article under the CC BY-NC-ND license (http://creativecommons.org/licenses/by-nc-nd/4.0/).

From the [a]Laboratory of Cardio-Oncology and Medicinal Chemistry, CNRS (FRE2033), Illkirch, France; [b]Institute of Biomedical Sciences, Academia Sinica, Taipei, Taiwan; [c]FRIM UMS37, Hospital Bichat assistance public-Paris Hospital, University of Paris Diderot, PRES Paris Cité, DHU FIRE, Inserm U1138, Paris, France; [d]Institute of Structural Biology, Helmholtz Zentrum München-German Research Center for Environmental Health (GmbH), Neuherberg, Germany; [e]Department of Biomedical Sciences, National Chung Cheng University, Chiayi, Taiwan; and the [f]European Institute of Oncology, Milan, Italy. This study was supported by

ISSN 2666-0873 https://doi.org/10.1016/j.jaccao.2019.06.003

Despite successful development of small molecules and targeted therapies over the last 15 years, anthracycline chemotherapy still plays a prominent role in many types of cancer treatment (1). However, doxorubicin (DOX), an anthracycline, significantly increases the risk of cardiomyopathy and heart failure (HF) (2).

A dose limitation strategy is used to reduce DOX-induced cardiovascular toxicity because DOX cardiotoxicity is dose-dependent (3). However, lower DOX doses may prohibit successful completion of chemotherapy and may still promote cardiovascular disorders, presenting a dilemma for both oncologists and cardiologists (4). The molecular and cellular mechanisms of dose-dependent, DOX-induced cardiovascular toxicity are not yet entirely understood (5). Moreover, there are few drugs that attenuate the cardiovascular toxicity of anticancer drugs (6).

SEE PAGE 103

Prokineticins (PROK1 and PROK2) are peptide hormones that are mainly released by macrophages (7). They exert their biological function via binding to 2 G-protein-coupled receptors (GPCRs), prokineticin receptors (PKR1 and PKR2; also known as PROKR1 and PROKR2, respectively). PROK2 is the most potent ligand for both receptors. PKR1 is mainly expressed in the peripheral nervous system, and PROK2 is primarily expressed in the central nervous system. PROK2 and PKR1 levels are altered in human patients with abdominal aortic rupture (8), during end-stage cardiac failure (9) after acute myocardial infarction (10), and in adipose tissues from obese human patients (11). *PKR1* gene transfer improves survival and heart function in a HF mouse model (12) and promotes coronary arteriogenesis and ischemia resistance (9). However, *PKR2* overexpression in cardiomyocytes promotes pathological cardiac hypertrophy and causes vascular leakage (13). Therefore, IS20, a non-peptide agonist specific for PKR1, was developed (14) to mimic the cardioprotective effects of PROK2.

Here, we studied how DOX dose- and time-dependency promotes damage in cardiomyocytes, endothelial cells (ECs), and human epicardium-derived progenitor cells (EDPCs). We hypothesized that PKR1 could be an interesting target for prevention of DOX-induced cardiovascular toxicity in vitro in cardiac cells and in vivo in mouse models of chronic and acute cardiotoxicity in breast cancer.

METHODS

Complete experimental details are available in the Methods section of the Supplemental Appendix.

STATISTICAL ANALYSIS. Data are expressed as mean ± SEM, except for murine experimental data, which are shown as mean ± SD. Statistical comparisons for terminal deoxynucleotidyl transferase deoxyuridine triphosphate nick end labeling (TUNEL), platelet endothelial cell adhesion molecule (PECAM)-1, calponin, smooth muscle actin-α, and kinase insert domain receptor staining on 40 heart cryosections obtained from 4 mice were performed using a 1-way analysis of variance with α-correction for pairwise comparisons using Tukey's method. Kaplan-Meier survival analysis (log-rank) was performed for 2 group comparisons. Statistical analyses for the murine experimental data were conducted using GraphPad Prism software, version 6.0 (GraphPad Software, La Jolla, California).

RESULTS

PKR1 ACTIVATION DIMINISHES DOX-MEDIATED APOPTOSIS IN H9C2 CARDIOMYOCYTES. To assess whether PKR1 signaling protects cardiomyocytes against DOX-mediated cardiotoxicity, viability assays were performed in H9c2 rat cardiomyocytes. The viability of H9c2 cardiomyocyte lines was significantly reduced by 1 μM DOX within 14 h (15). PROK2 and PKR1 agonist IS20 reversed this effect of DOX in a dose-dependent manner (**Figures 1A and 1B**).

The results of a TUNEL assay on the H9c2 cardiomyocyte line demonstrated that DOX (1 μM, 14 h) significantly increased apoptosis (**Figure 1C**), indicating that the reduced cell viability was due to apoptosis. Pre-treatment with 10 nM IS20 significantly reduced DOX-associated apoptosis of H9c2 cardiomyocytes in comparison with cardiomyocytes treated with DOX only (**Figure 1C** and histogram). The

ABBREVIATIONS AND ACRONYMS

DMSO = dimethyl sulfoxide

EC = endothelial cell

EF = ejection fraction

EDPC = epicardium-derived progenitor cell

FS = fractional shortening

GPCR = G-protein-coupled receptor

HAEC = human aortic endothelial cell

HF = heart failure

HFrEF = heart failure with reduced ejection fraction

MAPK = mitogen-activated protein kinase

NRF2 = nuclear factor, erythroid 2 like 2 (also known as NFE2L2)

PECAM = platelet and endothelial cell adhesion molecule

PKR1 = prokineticin receptor-1 (also known as PROKR1)

PKR1-KO = prokineticin receptor 1 knockout mice

PROK1 = prokineticin 1

PROK2 = prokineticin 2

TUNEL = terminal deoxynucleotidyl transferase deoxyuridine triphosphate nick end labeling

grants from European ERA-NET, ERA-CVD-JC2016, French government managed by Agence Nationale de la Recherche (ANR-16-ECVD-0005-01) Centre National de la Recherche Scientifique, Université de Strasbourg, and the Ministry of Science and Technology, Taiwan (MOST 104-2314-B-194). Dr. Tetko is CEO of BIGCHEM GmbH. All other authors have reported that they have no relationships relevant to the contents of this paper to disclose.

Manuscript received June 19, 2019; accepted June 27, 2019.

FIGURE 1 DOX (Medium Concentration)-Induced Cardiomyocyte Death Is Alleviated by PKR1 Signaling

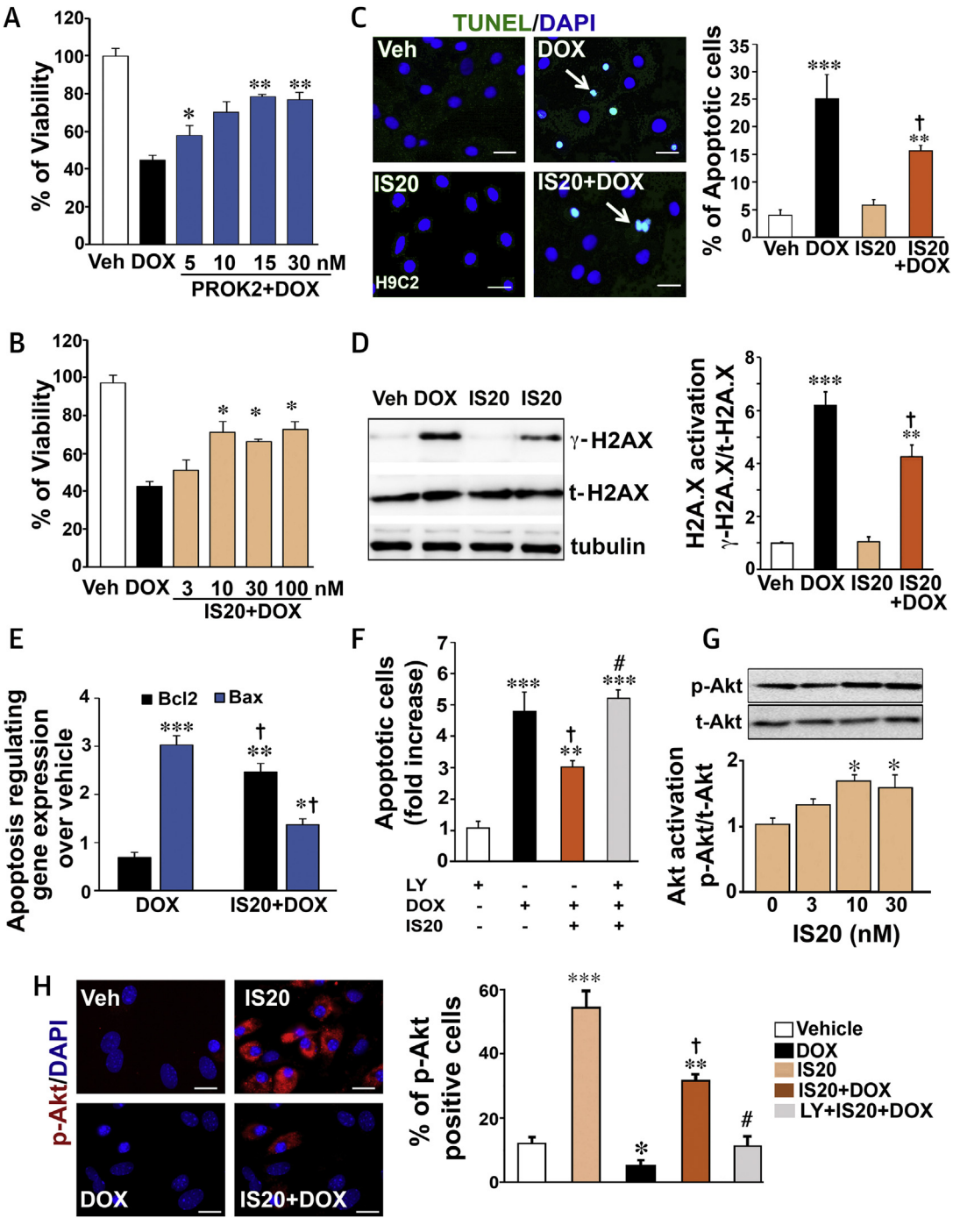

Continued on the next page

antiapoptotic effect of IS20 was reversed by pretreatment of cells with an antagonist of PKR1, PC25 (16), or by downregulation of the PKR1 gene by a short interfering RNA (siRNA) for PKR1 (siRNA-PKR1) (Supplemental Figures 1A and 1B) (9), indicating that IS20 specifically uses PKR1.

Because phosphorylation of histone H2AX at serine 139 (γ-H2AX) occurs in response to double-stranded

DNA breaks and is an early indicator of DNA damage (17), we used Western blots to characterize the DOX-induced apoptotic pathway in H9c2 cardiomyocytes by analyzing γ-H2AX in cell lysates. Exposure of H9c2 cardiomyocytes to 1 μM DOX for 14 h resulted in increased levels of γ-H2AX. This increase in γ-H2AX was attenuated by approximately 35% when H9c2 cardiomyocytes were pre-treated with IS20 (10 nM) (**Figure 1D** and histogram). In this setting, DOX decreased the expression ratio of the antiapoptotic gene B-cell lymphoma 2 (*Bcl2*)/proapoptotic gene BCL2-associated X (*Bax*), confirming that DNA breaks lead to apoptosis and that the IS20 pre-treatment prevented the dsDNA breaks (**Figure 1E**). The antiapoptotic effect of IS20 was diminished by pre-treatment of cells with an inhibitor of the phosphoinositide 3-kinase/serin threonin protein kinase B (Akt) pathway, LY294002 (1 μM, 1 h) (**Figure 1F**). IS20 activated AKT, a pro-survival kinase, by phosphorylation (p-AKT) within 10 min (**Figure 1G**). IS20 activation of AKT could also be observed in primary cardiomyocytes by p-AKT immunostaining (**Figure 1H**). DOX treatment decreased the number of p-AKT positive primary cardiomyocytes in the presence of IS20 (**Figure 1H**). The AKT activating effect of IS20 was mitigated by LY294002 (**Figure 1H** histogram), indicating that the antiapoptotic effect of PKR1 signaling was coupled to activation of AKT in H9c2 cardiomyocytes.

PKR1 ACTIVATION DIMINISHES DOX-MEDIATED PRODUCTION OF REACTIVE OXYGEN SPECIES. Several studies have shown that DOX-induced cardiotoxicity is also related to increases in oxidative stress and production of reactive oxygen species (ROS) (18). In the apoptosis induction protocol, DOX (1 μM for 14 h) did not induce any detectable ROS accumulation (Supplemental Figure 1C). Next, we exposed H9c2 or primary neonatal cardiomyocytes with different concentrations of DOX for a short period of time (e.g., 3 h) to detect ROS accumulation as an early oxidative event. DOX at 15 μM maximally increased ROS production by 3-fold within 3 h in primary and H9c2 cardiomyocytes (**Figure 2A**). Accordingly, cellular uptake of DOX in the H9c2 cardiomyocytes was detected when the cells were exposed to 15 μM DOX but not to 1 μM DOX. IS20 did not alter DOX uptake in these cells (Supplemental Figure 1D). PROK2 and IS20 suppressed the ROS production induced by DOX in a dose-dependent manner in both primary and H9c2 cardiomyocytes, respectively (**Figures 2B and 2C**). This ROS-suppressive effect of IS20 was completely reversed in the presence of the PKR1 antagonist PC25 (30 nM) (**Figure 2D**) in H9c2 cardiomyocytes, indicating that this effect was mediated by PKR1.

We questioned whether DOX and PKR1 signaling had any effect on the detoxification system, more specifically, activation of the redox-sensitive nuclear factor 2, erythroid like 2 (NRF2, also known as NFE2L2), which induces the expression of antioxidant and cytoprotective genes under stress conditions (19). Western blot (**Figure 2E** and histogram) and immunostaining (**Figure 2F**) analyses using an NRF2 antibody revealed that DOX treatment of H9c2 cardiomyocytes resulted in cytoplasmic accumulation of NRF2. However, IS20 pre-treatment resulted in translocation of NRF2 to the nucleus (**Figures 2E and 2F**).

FIGURE 1 Continued

(A) The rat H9C2 cardiomyocyte line was subjected to vehicle (Veh; phosphate buffered saline [PBS]) or doxorubicin (DOX) (1 μM 24 h) in the absence or presence of different concentrations of prokineticin-2 (PROK2, 10 h) to address the cardioprotective effect of the endogenous ligand of PKR1 (n = 3 to 5). **(B)** Same as in **A**, except cells were exposed to a chemical agonist of PKR1, IS20. **(C)** Terminal deoxynucleotidyl transferase deoxyuridine triphosphate nick end labeling (TUNEL) staining of apoptotic H9c2 cells treated with DOX (1 μM, 14 h) in the presence or absence of IS20 or vehicle (dimethyl sulfoxide [DMSO]). Confocal images of the TUNEL-positive **(green)** cell population in the total cell population (4′,6-diamidino-2-phenylindol [DAPI]-positive, **blue**) are shown in the **left panel**; quantitative analyses of images (250 to 400 cells across 3 independent experiments) are shown in the histogram **(right panel)**. Scale bar is 25 μm. **(D)** In the same setting as for TUNEL analyses **(C)**, cell lysates were probed with antibodies for phosphorylated H2A.X (γ-H2A.X) or total H2A.X (t-H2A.X) and tubulin **(left panel)**. The histogram **(right panel)** shows quantitative analyses of phosphorylated H2A.X, normalized by total H2A.X and tubulin (n = 4). **(E)** Quantitative reverse transcription polymerase chain reaction (qRT-PCR) quantification of the expression level of the apoptosis-regulating genes (*Bcl2* and *Bax*) over vehicle (n = 4 to 6). **(F)** Quantification of apoptotic cells in the same experimental setting as in **(C)**, with some cells pre-treated with the phosphoinositide 3 kinase (PI3K)/serin threonin protein kinase B (Akt) inhibitor LY294002 (LY; 1 μM) 1 h before IS20 and DOX treatments (n = 3 to 5). **(G)** Cell lysates from H9c2 cells treated with different concentrations of IS20 for 10 min were probed with AKT antibodies (phosphorylated [p-AKT] or total [t-AKT]) **(upper panel)**. The histogram at the **bottom** shows quantification of AKT activity from 3 to 4 independent experiments. **(H)** p-AKT immunostaining of primary neonatal cardiomyocytes treated as in **B**. Confocal images of the p-AKT-positive (red) cell population with the total cell number (DAPI-positive, **blue**) shown in the **right panel** and quantitative analyses of images (250 to 400 cells across 3 independent experiments) in the histogram **(right panel)**. Scale bar is 50 μm. All data are presented as mean ± SEM. *p < 0.05, **p < 0.01, and ***p < 0.001 versus vehicle; †p < 0.05 versus DOX; #p < 0.05 versus IS20 + DOX. Source data for this figure are available in the Supplemental Appendix.

FIGURE 2 DOX (High Concentration)-Induced ROS production in Cardiomyocytes Mitigated by PKR1 Signaling

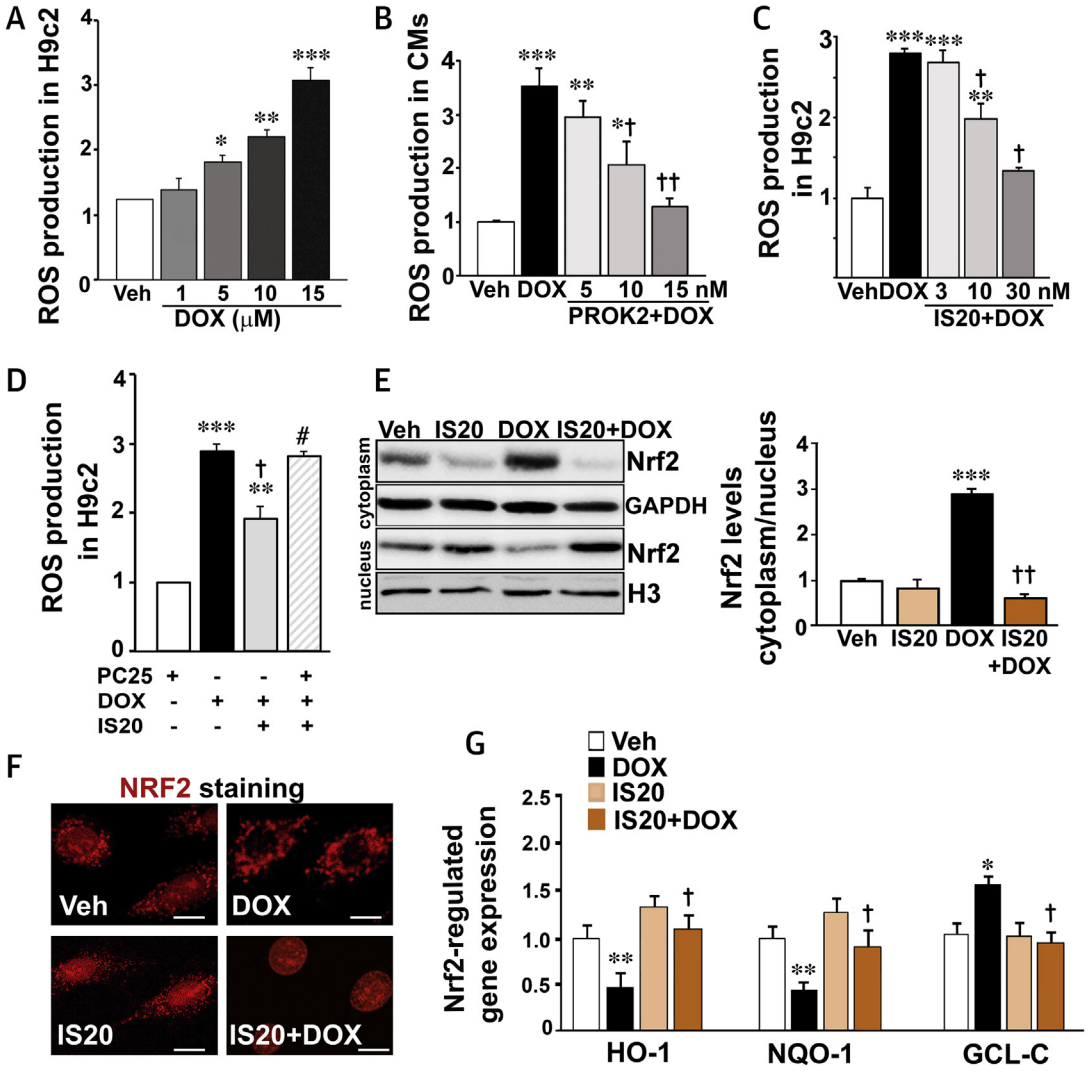

(A) Different concentration of DOX-mediated ROS accumulation in H9c2 cardiomyocytes. **(B)** Primary cardiomyocytes were subjected to vehicle (PBS) or DOX (15 μM, 3 h) in absence or presence of different concentrations of PROK2 and ROS production was detected by 2',7'-dichlorofluorescin diacetate (DCFDA; n = 4). **(C)** H9c2 cells were subjected to vehicle (0.1% DMSO) or DOX (15 μM 3 h) in absence or presence of different concentrations of IS20 (16 h), and ROS production was detected by DCFDA (n = 4). **(D)** ROS production was detected by DCFDA in H9c2 cells treated as in **C**, some cells pre-treated with the PKR1 inhibitor PC25 (30 nM) 1 h before IS20 and DOX treatments (n = 4). **(E)** Cytosolic and nuclear cell lysates from H9C2 cells treated as in **B** were probed with the indicated antibodies **(left panel)**. The histogram shows quantification of nuclear versus cytoplasmic NRF2 (n = 3). **(F)** Immunostaining of H9c2 cells with NRF2 antibody after treatments as in **B** (n = 3). Scale bar is 50 μm. **(G)** qRT-PCR quantification of the expression levels of NRF2-regulated genes (*Hmox1*, *Nqo1*, *Gclc*) in H9c2 cells treated as in **B** from 3 to 5 independent experiments. All data are expressed as mean ± SEM. *p < 0.05, **p < 0.01, and ***p < 0.001 versus vehicle; †p < 0.05 and ††p < 0.01 versus DOX; #p < 0.05 versus IS20 + DOX, n = 3 to 4 hearts for each group. Source data for this figure is available in the Supplemental Appendix. GAPDH = glyceraldehyde 3-phosphate dehydrogenase; *Gclc* = γ-glutamyl cysteine synthetase catalytic subunit; H3 = histone H3; *Hmox1* = heme oxygenase 1; *Nqo1* = NAD(P)H quinone oxidoreductase 1; ROS = reactive oxygen species; other abbreviations as in Figure 1.

The NRF2-regulated expression of antioxidant and detoxificant genes, such as heme oxygenase 1 *(Hmox1),* a stress response gene, and nicotinamide adenine dinucleotide phosphate hydrogen (NAD(P)H) quinone dehydrogenase 1 *(Nqo1)*, a reduction enzyme, were both reduced by DOX, whereas the glutamate-cysteine ligase catalytic subunit (*Gclc*), involved in synthesis of glutathione, was increased.

FIGURE 3 IS20 Prevents DOX-Induced Impairments in the ECs and hEPDCs

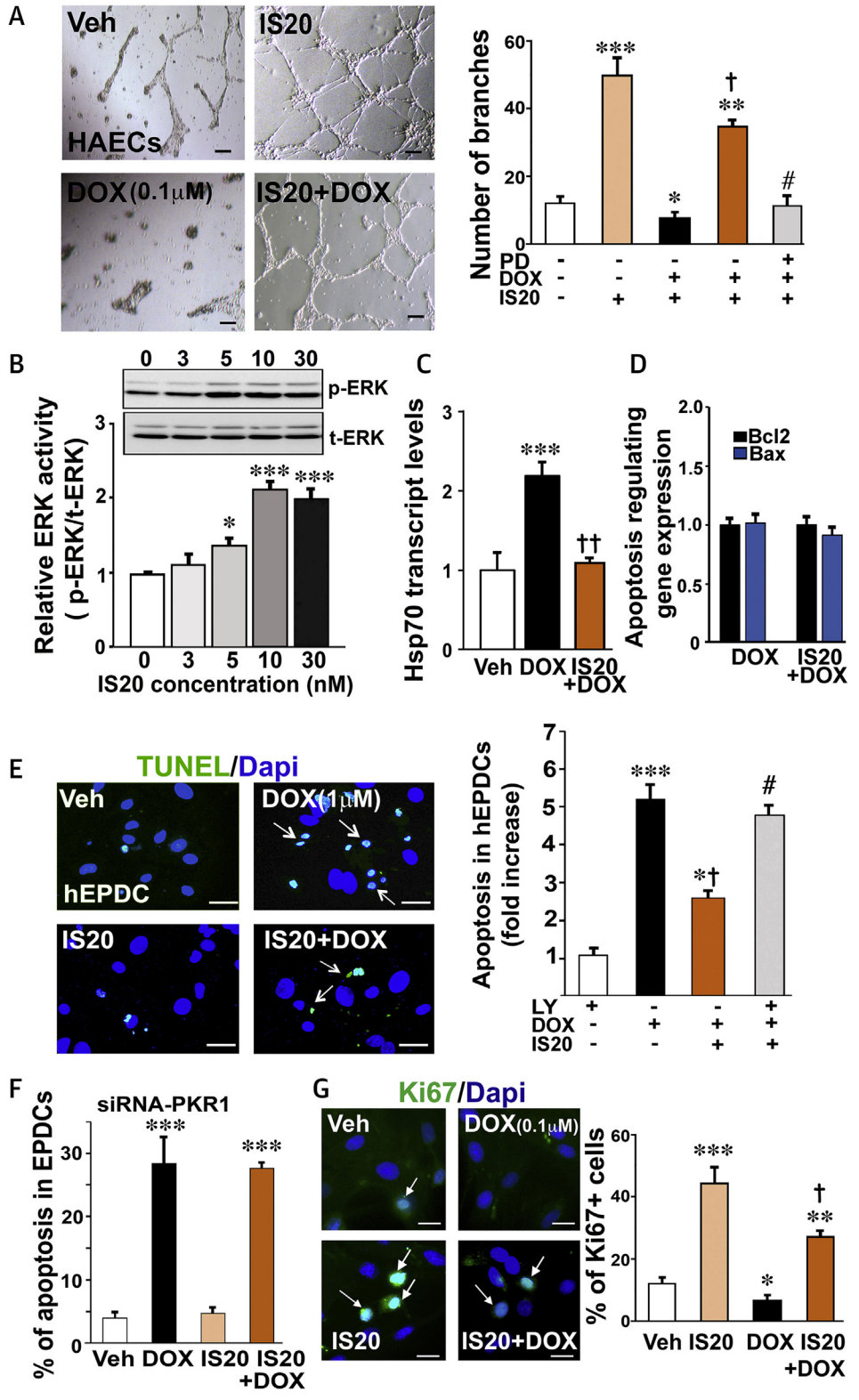

Continued on the next page

All these effects of DOX were counteracted by IS20 in H9c2 cardiomyocytes (**Figure 2G**). In this setting, DOX did not alter the ratio of *Bcl2*/*Bax* gene expression (Supplemental Figure 1E). These data indicated that DOX at high concentration induced ROS accumulation in cardiomyocytes, inhibiting the oxidative stress clearance systems. These effects of DOX were counteracted by activation of PKR1 signaling.

EFFECT OF IS20 ON ENDOTHELIAL AND PROGENITOR CELLS IN DOX-TREATED HEARTS. To investigate whether DOX disrupted EC function, in vitro angiogenesis was performed on human aortic endothelial cells (HAECs) in the presence or absence of DOX. IS20, like PROK2 (20), promoted the formation of tube-like structures by HAECs cultured on Matrigel (Fisher Scientific, Illkirch-Graffenstaden, France) (**Figure 3A**). Treatment of the HAECs with DOX at a low concentration (0.1 μM, 14 h) substantially inhibited basal tube formation; however, tube formation was restored by IS20 pre-treatment (**Figure 3A** and histogram). Pre-treatment of cells with the mitogen-activated protein kinase (MAPK) inhibitor PD98056 (1 μM) blocked this effect of IS20 (**Figure 3A** histogram). These data were consistent with an effect of IS20 on MAPK activation by phosphorylation in HAECs (**Figure 3B**). We also observed upregulation of heat shock protein 70 (*HSP70*), an indicator of EC dysfunction (21), in DOX-treated but not IS20 + DOX-treated HAECs (**Figure 3C**). However, in this setting, the *BCL2*/*BAX* transcription ratio remained unchanged by DOX (**Figure 3D**). It should be noted that DOX, even at 0.3 μM for 14 h, did not significantly induce apoptosis, as detected by the TUNEL assay (12 ± 7%) compared with that in the vehicle-treated HAECs (8 ± 3%). However, 1 μM DOX did promote apoptosis in HAEC cells within 14 h, which was attenuated by IS20 (Supplemental Figure 2A). Pre-treatment of cells with the MAPK inhibitor PD98056 (1 μM) inhibited the antiapoptotic effect of IS20 (Supplemental Figure 2A).

To assess whether different doses of DOX induced apoptosis and altered the function of EDPCs, human EDPCs were exposed to DOX. After 14 h, DOX at 1 μM increased apoptosis by approximately 7-fold. Pre-treatment of human EDPCs with IS20 (10 nM) reduced DOX toxicity by 4-fold (**Figure 3E** and histogram), which could be reversed using the phosphoinositide 3-kinase/AKT inhibitor LY294002 (1 μM) (**Figure 3E** histogram). This effect of IS20 was mediated by PKR1 because IS20 had no antiapoptotic effect when PKR1 was downregulated using siRNA-PKR1 in EDPCs (**Figure 3F**). This protective effect of IS20 was similar to that of PROK2 (10 nM) against DOX toxicity in human EDPCs (Supplemental Figure 2B). However, DOX at 0.1 μM inhibited basal and IS20-mediated Ki67-positive cell proliferation, which indicated that DOX at low concentration inhibited the plasticity of human EDPCs (**Figure 3G** and histogram). Taken together, these data demonstrated that a low concentration of DOX impaired EC and EDPC function at the expense of apoptosis.

IS20 PROTECTS THE HEART AGAINST DOX CARDIOTOXICITY IN VIVO. Using in silico analysis, the median lethal dose (900 mg/kg) and lowest effect level to induce in vivo toxicity (170 mg/kg) were predicted for intraperitoneal administration of IS20 in mice. The half-life of IS20 (0.5 mg/kg) in vivo was predicted to be approximately 10 h. Thus, we used 1 mg/kg of IS20 intraperitoneally in the in vivo assays.

Next, to examine whether IS20 at 1 mg/kg activated the AKT survival pathway in the mouse hearts, we injected wild-type and PKR1 knockout (PKR1-KO)

FIGURE 3 Continued

(A) Human aortic endothelial cells (HAECs) were subjected to vehicle (0.1% DMSO) or DOX (0.1 μM, 14 h) 10 h after IS20 pre-treatment on Matrigel. **(Left)** Images and **(right)** quantification of tube formation of HAECs on Matrigel after treatment histogram. Pre-treatment of the cells with PD98056 (1 μM) before IS20 pre-treatment completely blocked the effect of IS20 (6 wells from 3 different experiments). **(B)** Cell lysates from HAECs treated with different concentration of IS20 for 10 min were probed with extracellular signal-related kinase (ERK1/2) antibodies **(left panel)**. Quantification of phosphorylated ERK1/ERK2 (p-ERK) normalized by total ERK1/ERK2 (t-ERK) is shown in the **bottom panel** (n = 3). **(C)** qRT-PCR quantification of the expression level of the heat shock protein 70 (*Hsp70*) as a marker of endothelial dysfunction from 3 to 6 independent experiments in the settings described in **A** (n = 3). **(D)** qRT-PCR quantification of the expression level of the apoptosis-regulating genes (*BCL2* and *BAX*) from 3 to 6 independent experiments in the settings described in **A** (n = 3). **(E)** TUNEL staining of apoptotic human epicardial progenitor cells (hEPDCs) treated with DOX (1 μM, 14 h) in the presence or absence of IS20 or vehicle (DMSO). Confocal images of TUNEL positive **(green)** cell population in the total cell population (DAPI-positive, **blue**) are shown on the **left**, and quantitative analyses of images (250 to 400 cells across 3 independent experiments) are shown in the histogram **(right)**. Scale bar is 25 μm. **(F)** Same as in **E,** but the *PKR1* gene was downregulated by short interfering RNAs (siRNAs) in EDPCs. **(G)** Ki67 staining of proliferating hEPDCs treated with DOX (0.1 μM, 14 h) in the presence or absence of IS20 or vehicle (DMSO). Confocal images of Ki67 positive **(green)** cell population in total cell number (DAPI-positive, **blue**) are shown in the **left panel**, quantitative analyses of images (250 to 400 cells across 3 independent experiments) appear in the histogram **(right panel)**. Scale bar is 50 μm. All data are expressed as mean ± SEM. *$p < 0.05$, **$p < 0.01$, and ***$p < 0.001$ versus vehicle; †$p < 0.05$ and ††$p < 0.01$ versus DOX; # $p < 0.05$ versus IS20 + DOX. Source data for this figure are available in the Supplemental Appendix. EC = endothelial cell; other abbreviations as in **Figure 1**.

FIGURE 4 **IS20 Protects Hearts in the Chronic Model of DOX Cardiotoxicity**

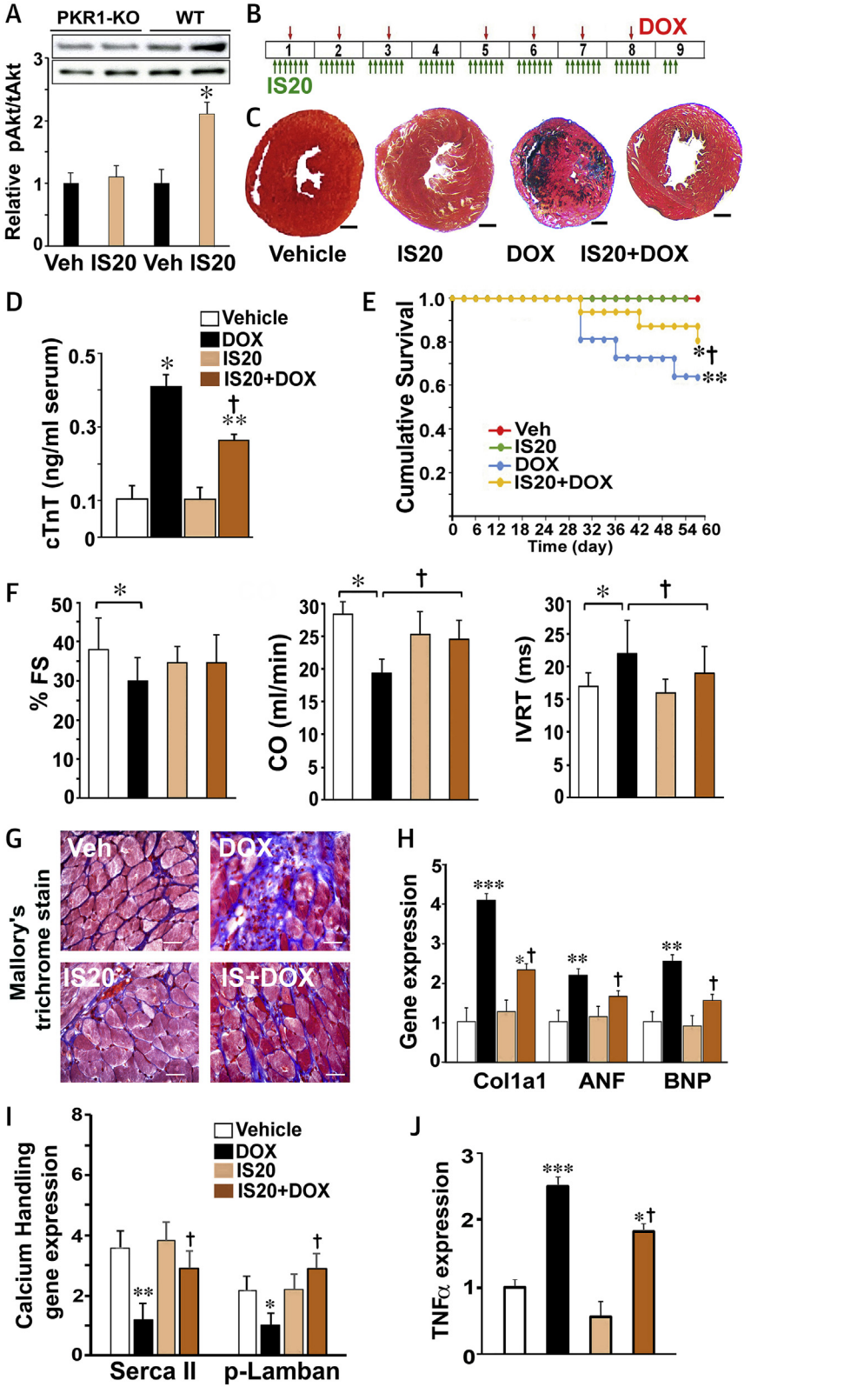

Continued on the next page

JACC: CARDIOONCOLOGY, VOL. 1, NO. 1, 2019
SEPTEMBER 2019:84–102

TABLE 1 Echocardiographic Analyses in the Mouse Chronic Toxicity Model

	Vehicle (n = 10)	IS20 (n = 11)	DOX (n = 13)	DOX + IS20 (n = 17)
Heart rate (beats/min)	512 ± 19	506 ± 22	436 ± 11*	457 ± 18*
LA/BW (mm/g)	0.08 ± 0.01	0.08 ± 0.01	0.10 ± 0.02*	0.09 ± 0.02
LVESD (mm)	2.60 ± 0.44	2.73 ± 0.31	2.99 ± 0.52	2.85 ± 0.4
LVEDD (mm)	4.19 ± 0.31	4.08 ± 0.24	4.1 ± 0.46	4.18 ± 0.40
LVEDe D/BW (mm/g)	0.14 ± 0.01	0.13 ± 0.01	0.18 ± 0.02*	0.18 ± 0.02*
LV systolic function				
EF (%)	75 ± 16	71 ± 6	65 ± 9*	69.5 ± 3.7
Sa (cm/s)	2.72 ± 0.8	2.33 ± 0.8	1.77 ± 0.7*	2.03 ± 0.6*
Spw (cm/s)	2.67 ± 0.4	2.52 ± 0.4	2.08 ± 0.6*	2.16 ± 0.5*
LV diastolic function				
E′a (cm/s)	3.8 ± 1.2	3.28 ± 1	2.46 ± 0.8*	2.68 ± 1*†
E′pw (cm/s)	3.5 ± 1	3.1 ± 0.7	2.3 ± 0.7*	3.0 ± 1 t

Values are mean ± SD. *p < 0.05 vs. vehicle. †p < 0.05 vs. doxorubicin (DOX).

BW = body weight; DOX = doxorubicin; E′a = diastolic velocity of mitral annulus; E′pw = diastolic velocity of posterior wall; EF = ejection fraction; IVRT = isovolumic relaxation time; LA = left atrium; LVEDD = left ventricular end-diastolic diameter; LVESD = left ventricular end-systolic diameter; Sa = systolic velocity of mitral annulus; Spw = systolic velocity of posterior wall.

mice with IS20 (intraperitoneally, 1 mg/kg) or vehicle (0.1% dimethyl sulfoxide [DMSO]). IS20 at 1 mg/kg activated AKT within 20 min in the wild-type murine hearts but not in the PKR1-KO hearts (Figure 4A), indicating a PKR1-mediated effect in vivo.

To analyze the effects of IS20 in a mouse model of chronic DOX cardiotoxicity, we injected (intraperitoneally) mice with IS20 (1 mg/kg) or vehicle (0.1% DMSO) every day for 9 weeks. These mice received DOX (5 mg/kg) once a week for 7 weeks with 2 intervals using a similar set of protocols to those used clinically (Figure 4B).

Animals treated with DOX showed weight loss in comparison with the vehicle control group (Supplemental Figure 3). IS20 slightly improved the loss of weight in DOX-treated mice. IS20 itself had no effect on the body weight of the mice. DOX-only treated mice had no pleural effusion or lung edema.

The average heart weight of the DOX-treated mice after 9 weeks of the protocol (120 ± 8 mg vs. vehicle and IS20 + DOX; p < 0.05) was the lowest among the 4 groups of hearts (vehicle: 150 ± 10 mg; IS20: 165 ± 12 mg; IS20 + DOX: 140 ± 9 mg) as observed in another model of DOX-mediated cardiotoxicity (22). Histological sections also confirmed that DOX-treated mice had the smallest heart diameters, as shown in Figure 4C.

The cardiac toxicity in DOX-treated mice was evident from their elevated serum levels of the cardiac damage biomarker cardiac troponin T (Figure 4D). IS20 reduced this cardiotoxicity marker in DOX-treated mice. The survival rates of mice in the vehicle and IS20 alone group were 100%. After the first interval, DOX-treated animals had a compromised survival rate (60.7%). IS20 cotreatment increased the survival rate by 28% compared with the DOX-only group (Figure 4E).

To assess how these alterations in cardiotoxicity biomarkers were associated with heart function, we performed Doppler echocardiography (Table 1). Left ventricular function was not affected by treatment with IS20 alone. However, DOX-treated mice had substantial deterioration of cardiac function characterized by significant enlargement of the left atrium, increased left ventricular diameter as indexed to body weight, reduced left ventricular fractional shortening (FS) (Figure 4F) and ejection fraction (EF) compared with vehicle-treated mice (Table 1). Impairments in isovolumic relaxation time and E′ tissue Doppler at the mitral annulus and posterior wall (Sa and Spw) indicated severe left ventricular diastolic dysfunction in the DOX-treated hearts. We observed improved cardiac output, isovolumic relaxation time, and E′pw in animals cotreated with IS20 compared with those that received DOX alone (Figure 4F, Table 1). The IS20 + DOX group had a clear trend toward improved FS and EF compared with the DOX-only group (Figure 4F, Table 1).

FIGURE 4 Continued

(A) AKT activation by phosphorylation in heart tissue lysates from wild type and prokineticin receptor-1 knockout (*Pkr1*-KO) mice 20 min after intraperitoneal injection of IS20 (1 mg/kg) or vehicle. **(B)** Illustration of the chronic cardiotoxicity protocol in mice. **(C)** Images of Mallory trichrome staining of cryo-sectioned hearts. Scale bars are 2.5 μm. **(D)** Serum cardiac troponin T (TNNT2) levels as a marker of heart damage from mice in the indicated groups (n = 6). **(E)** Cumulative survival analysis, as determined by the Kaplan-Meier plot, shows a significant difference in survival curves between the DOX group (n = 20) and the IS20 + DOX group (n = 20) (p = 0.028 by the log-rank test). **(F)** Echocardiographic analyses showing fractional shortening (FS), cardiac output (CO), and isovolumic relaxation time (IVRT) in mice treated with vehicle (Veh, 0.1% DMSO), IS20, PKR1 prokineticin receptor 1 (PKR1) agonist, DOX and IS20 + DOX. Data are expressed as mean ± SD for echocardiographic analyses. **(G)** Examples of Mallory trichrome staining of cryo-sectioned hearts. **Blue** indicates fibrosis. **(H)** qRT-PCR analyses of the expression of cardiac remodeling genes (*Col1a1*, *ANF*, and *BNP*). **(I)** qRT-PCR analyses of contractility regulating calcium handling genes (SERCA2 [*Atp2a2*], phospholamban [*Pln*]) (n = 4). **(J)** Levels of the tumor necrosis factor-α (*Tnf*) transcript, an indicator of necrosis (n = 4). All data are expressed as mean ± SEM, except for echocardiographic analyses. *p < 0.05, **p < 0.01, and ***p < 0.001 versus vehicle; †p < 0.05 versus DOX. ANF = atrial natriuretic factor; BNP = B-type natriuretic peptide, n = 4. COL1a1 = collagen type 1a1; other abbreviations as in Figure 1.

FIGURE 5 Molecular Mechanism of DOX Cardiotoxicity and Cardioprotection by IS20

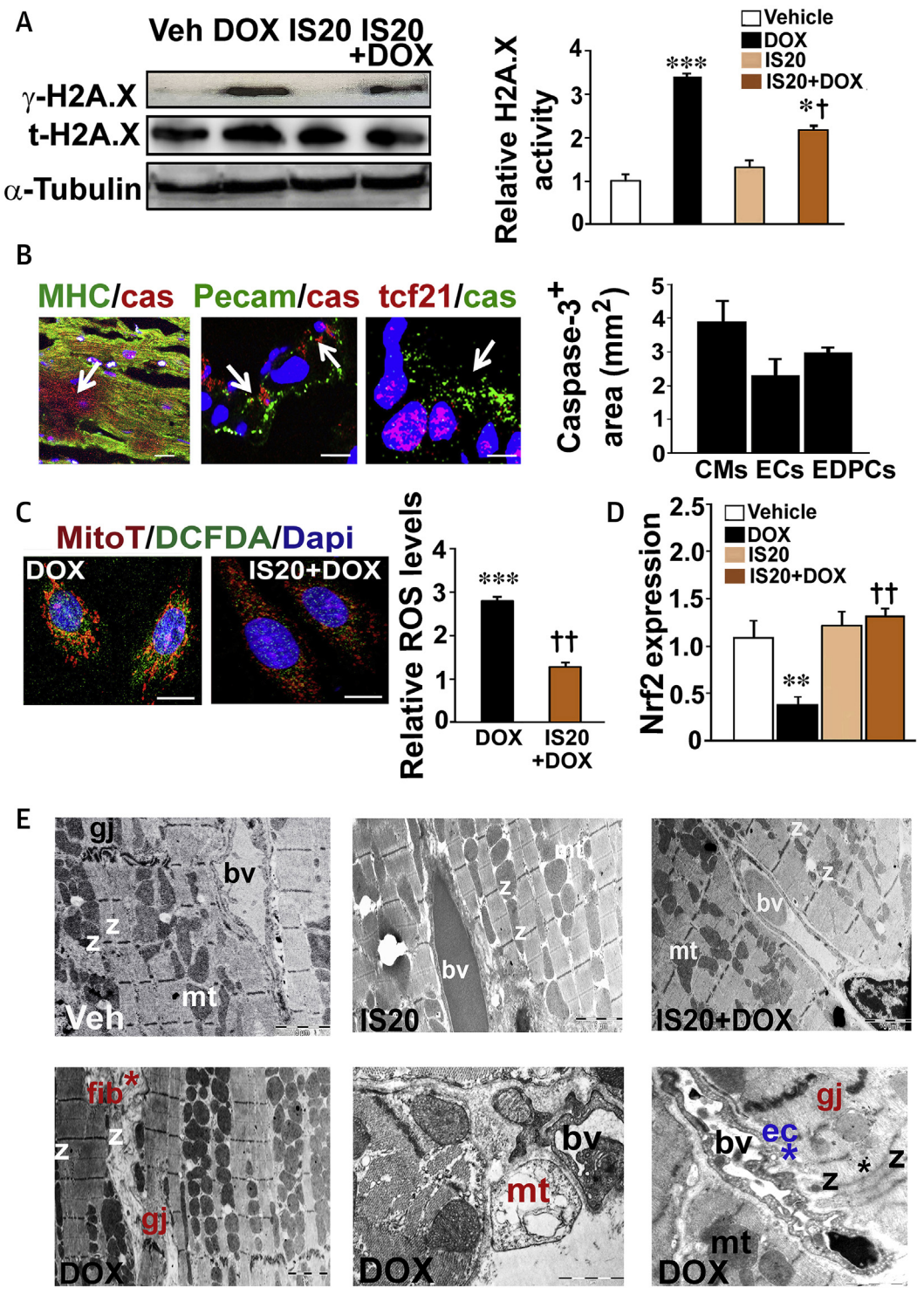

Continued on the next page

Mallory's trichrome staining of heart sections revealed severe fibrosis (blue) in DOX-treated hearts (**Figure 4G**). Quantitative polymerase chain reaction analyses of the mouse hearts demonstrated elevated expression of pathological remodeling genes, such as collagen (*Col1a1*), natriuretic peptide A (*Nppa*), atrial natriuretic factor (ANF), and natriuretic peptide B (*Nppb*), in hearts treated with DOX only (**Figure 4H**). IS20 cotreatment reduced these transcript levels.

The reduced levels of calcium-handling genes (*SERCA2* [*Atp2a2*] and phospholamban [*Pln*]) in the hearts treated with DOX only confirmed the cardiac contractility dysfunction and were also restored by IS20 treatment (**Figure 4I**). An elevated level of the tumor necrosis factor-α (*Tnf*) transcript, an indicator of necrosis, was also reduced by IS20 treatment in the DOX-treated mice (**Figure 4J**).

IS20 RESTORES DOX-MEDIATED PATHOLOGICAL CARDIAC REMODELING IN DOX-TREATED HEARTS. To determine if replacement fibrosis occurred following apoptosis induction by DOX, as observed in cancer patients (23), we compared the phosphorylation of the histone H2AX in the heart lysates. Mice cotreated with IS20 and DOX exhibited a decrease in cardiac γ-H2AX levels compared with those in animals treated with DOX only (**Figure 5A** and histogram**)**. Costaining of heart sections with antibodies for a marker of mitochondrial apoptosis, caspase-3, and cardiomyocyte-specific myosin heavy chain, an endothelial-specific platelet and endothelial cell adhesion molecule (PECAM)-1, or an epicardial-specific transcription factor-21 showed that cardiomyocytes, ECs, and epicardial cells were damaged in the long-term DOX-treated hearts (**Figure 5B** and histogram).

Next, we compared the levels of ROS in the cardiomyocytes isolated from the DOX-only and IS20 and DOX cotreated hearts (in which DOX had already accumulated) in response to external DOX at a low concentration (0.1 μM) that did not induce ROS accumulation in the cardiomyocytes derived from vehicle- or IS20-treated hearts. The cardiomyocytes of IS20 and DOX cotreated mice stained with 2′,7′-dichlorofluorescin diacetate showed decreased intensity of ROS production in mitochondria labeled with MitoTracker (Red CMXRos, ThermoFisher, Illkirch, France) (**Figure 5C** and histogram). We also found reduced NRF2 expression in the hearts treated only with DOX (**Figure 5D**).

Electron microscopic analyses revealed that hearts treated with DOX only had severe collagen deposition and fibrosis (**Figure 5E**, lower left). Cytoplasmic vascularization, unevenly spaced microfibrils with nonuniform sarcomeres, recurrent Z bands, and round, swollen mitochondria with disorganized cristae were observed in the DOX-only treated hearts (**Figure 5E**, lower middle). The development of endothelial fenestration with vacuoles and degradation of the vascular basement membrane were evident in DOX-only treated hearts (**Figure 5E**, lower right**)**. These abnormalities were not observed in the vehicle- or IS20-treated hearts (**Figure 5E**, upper middle). Hearts treated with IS20 together with DOX had intact myofibers and vascular structures, as well as less fibrosis and abnormal mitochondrial structures (**Figure 5E**, upper right).

IS20 IMPROVES THE NUMBER OF VASCULAR NETWORKS AND EDPCS IN DOX-TREATED HEARTS. To verify the electron microscopic analyses, cryosectioned hearts were costained for endothelial-specific PECAM1 and smooth muscle-specific calponin. Hearts treated with DOX only exhibited severe structural instability, marked by detachment of the PECAM1-positive endothelial layer from calponin$^+$ pericytes/smooth muscle cells (**Figure 6A**). DOX-only treatment reduced calponin$^+$ vascular numbers by

FIGURE 5 Continued

(A) Western blotting analyses for H2AX protein phosphorylation (γ-H2AX) on samples from mouse hearts; (n = 6). Histogram shows quantitative analyses of γ-H2AX, normalized by total H2AX or tubulin. **(B)** Examples of heart sections costained for caspase-3 and myosin heavy chain (MHC; cardiomyocytes [CM]), platelet endothelial cell adhesion molecule (PECAM1; ECs) or transcription factor 21 (epicardial progenitor cells) antibodies. The histogram shows the relative caspase-3–positive apoptotic area in each image using a dedicated ImageJ (NIH) plugin (n = 20 to 50). **(C)** Cardiomyocytes isolated from DOX or IS20 + DOX treated hearts were stained with MitoTracker Red and DCFDA in response to DOX (0.1 μM) to assess ROS production in mitochondrial structures **(left panels)**. Scale bar is 50 μm. Relative ROS levels **(green)** were quantified on thresholder images using a dedicated ImageJ plugin. Quantification of ROS production is shown on the **left** histogram (n = 20 to 50). **(D)** qRT-PCR analyses of NRF2 expression in mouse hearts. **(E)** Electron microscope (EM) analyses in the hearts. Hearts treated with DOX only **(lower left)** demonstrate fibrosis (fib), fused myofibrillar structures with disorganized Z bands (z), swollen and permeabilized mitochondria (mt) with abnormal cristae **(upper right)**, abnormal ECs (ec*) in the blood vessels (bv), and disrupted gap junctions (gj) (n = 4 hearts/group). All data are expressed as mean ± SEM. *p < 0.05, **p < 0.01, and ***p < 0.001 versus vehicle; †p < 0.05 and ††p < 0.01 versus DOX. n = 4 to 6 mice/group. Source data for this figure are available in the Supplemental Appendix. Abbreviations as in **Figures 1** and **3**.

FIGURE 6 IS20 Restores Impaired Vascular Structure, Capillary and Vascular Density and hEPDC Deficits in DOX-Treated Mice

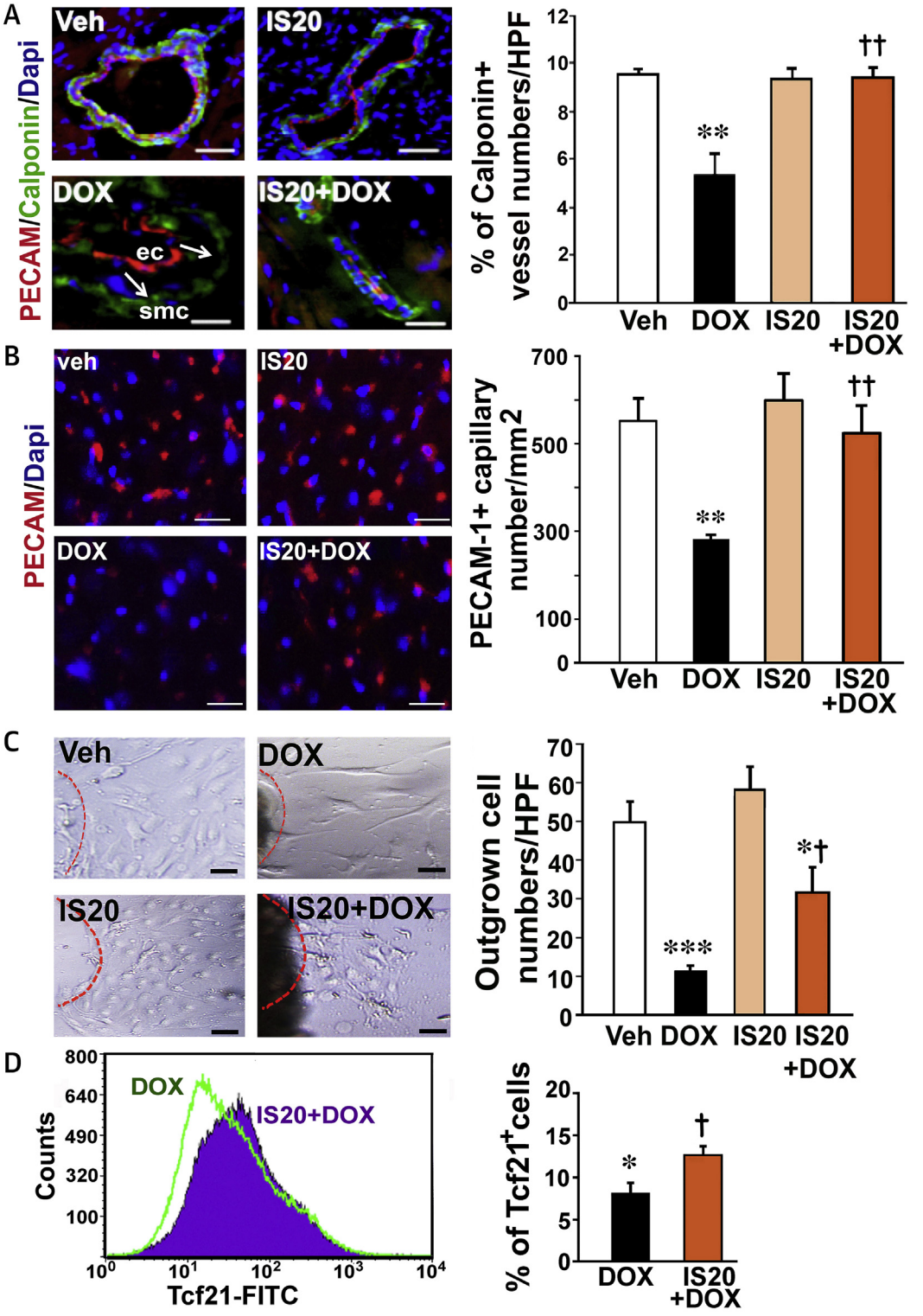

Continued on the next page

approximately 35%, which was reversed by IS20 administration (**Figure 6A** and histogram**)**. DOX also destroyed the capillary network, as detected by PECAM-1$^+$ cell numbers (**Figure 6B** and histogram). Hearts treated with IS20 only exhibited no significant alterations in capillary and vascular numbers. However, the IS20 and DOX cotreated group displayed a similar number of capillaries to that observed in the vehicle-treated group.

To test whether DOX-mediated cardiotoxicity could also be attributed to damage in cardiac progenitor/stem cells, EDPCs from epicardial explants were isolated from each group of mouse hearts. However, outgrown cells from epicardial explants were severely diminished in the DOX-treated hearts. IS20 cotreatment with DOX significantly recovered the numbers of outgrown cells (**Figure 6C** and histogram) and transcription factor 21$^+$ cells detected by fluorescence-activated cell sorting analyses of the hearts (**Figure 6D** and histogram).

IS20 DOES NOT INTERFERE WITH THE CYTOTOXIC ACTIVITY OF DOX ON BREAST AND OVARIAN CANCER CELLS. To assess whether IS20 interferes with the cytotoxic action of DOX, PKR1-expressing MDA-MB-231 and MC7 breast cancer cells were concurrently exposed to increasing doses of DOX and a constant concentration of either 10 nM or 1 μM IS20. IS20 did not interfere with the cytotoxic action of DOX at the assessed doses in the MDA-MB-231 and MC7 breast cancer cell lines (**Figures 7A and 7B**). IS20 also did not alter the cytotoxic effect of DOX on MDA-MB-453 breast and Kuramochi ovarian cancer cells (Supplemental Figures 4A and 4B). IS20 had no effect on the proliferation of these cancer cells.

IS20 PROTECTS THE HEART WITHOUT ALTERING THE ANTITUMOR ACTIVITY OF ACUTE DOX TREATMENT ON XENO-TRANSPLANTED MICE. To examine the effect of IS20 on the antitumor effect of acute DOX in vivo, we used a mouse model of breast cancer. We implanted breast cancer (MDA-MB-231) cells subcutaneously into athymic nude mice (BALB/cByJNarl). After tumor growth to a volume of approximately 20 mm^3, the mice received intraperitoneal injections of DMSO (control mice), DOX (5 mg/kg), or DOX + IS20 (1 mg/kg), as shown in **Figure 7C**. The presence of cardiac alterations was examined by cardiac magnetic resonance before and after the experiment. Tumor size and volume were measured when the mice were killed (**Figure 7D**). DOX significantly reduced the tumor size, whereas IS20 administration did not affect the tumor-inhibitory effects of DOX (**Figure 7E**).

Using this model, we found by cardiac magnetic resonance that DOX treatment of mice significantly promoted left ventricular end-diastolic volume defects, but that these defects were reversed by IS20 (Supplemental Figure 5A). To verify whether acute DOX treatment induced severe diastolic volume defects without mortality and to determine if this effect was due to the genetic background of the mouse strain, we used mouse models of acute cardiotoxicity in C57BL/6J mice. These mice were exposed to DOX (5 mg/kg, intraperitoneally once per week) for only 2 weeks, then subjected to cardiac magnetic resonance analyses (**Figure 7F**). **Figures 7G** (images) and 7H (middle panel) show that acute DOX-only treatment induced a severe decrease in diastolic volume without significantly altering systolic volume, and IS20 (1 mg/kg, intraperitoneal injections daily for 2 weeks) significantly alleviated diastolic volume defects in mice cotreated with DOX. Interestingly, left ventricular EF was not significantly altered in the DOX-only treated mice (**Figure 7H**, right panel). These left ventricular diastolic volume defects were also detectable by cardiac magnetic resonance 1 week after DOX treatment (Supplemental Figure 5B).

These data showed that DOX induced volume declines in both mouse strains without altering the EF, and activation of PKR1 by IS20 did not inhibit the antitumor activity of DOX but improved diastolic volume defects induced by acute DOX administration.

FIGURE 6 Continued

(A) Representative example of PECAM1 and calponin costaining in the cryo-sectioned hearts. **Arrow** shows detachment of ECs from smooth muscle cells (SMC). Quantification of calponin$^+$ vessel numbers is shown in the histogram. **(B)** Representative example and quantification of PECAM1 stained hearts in each group. n = 50 from 4 mice. **(C)** Example and quantification of outgrown cells from epicardial explants. n = 15 explants from 3 mice for each group. **(D)** Illustration of transcription factor-21 fluorescein isothiocyanate (FITC$^+$) fluorescence-activated cell sorting (FACS) and quantification of cells in DOX- and IS20 + DOX-treated mouse hearts in histogram. n = 3. All data are expressed as the mean ± SEM. *p < 0.05, **p < 0.01 and ***p < 0.001 versus vehicle; †p < 0.05 and ††p < 0.01 versus DOX. Abbreviations as in **Figures 1** and **5**.

FIGURE 7 **IS20 Did Not Interfere With the Cytotoxic Effects of DOX In Vitro and In Vivo**

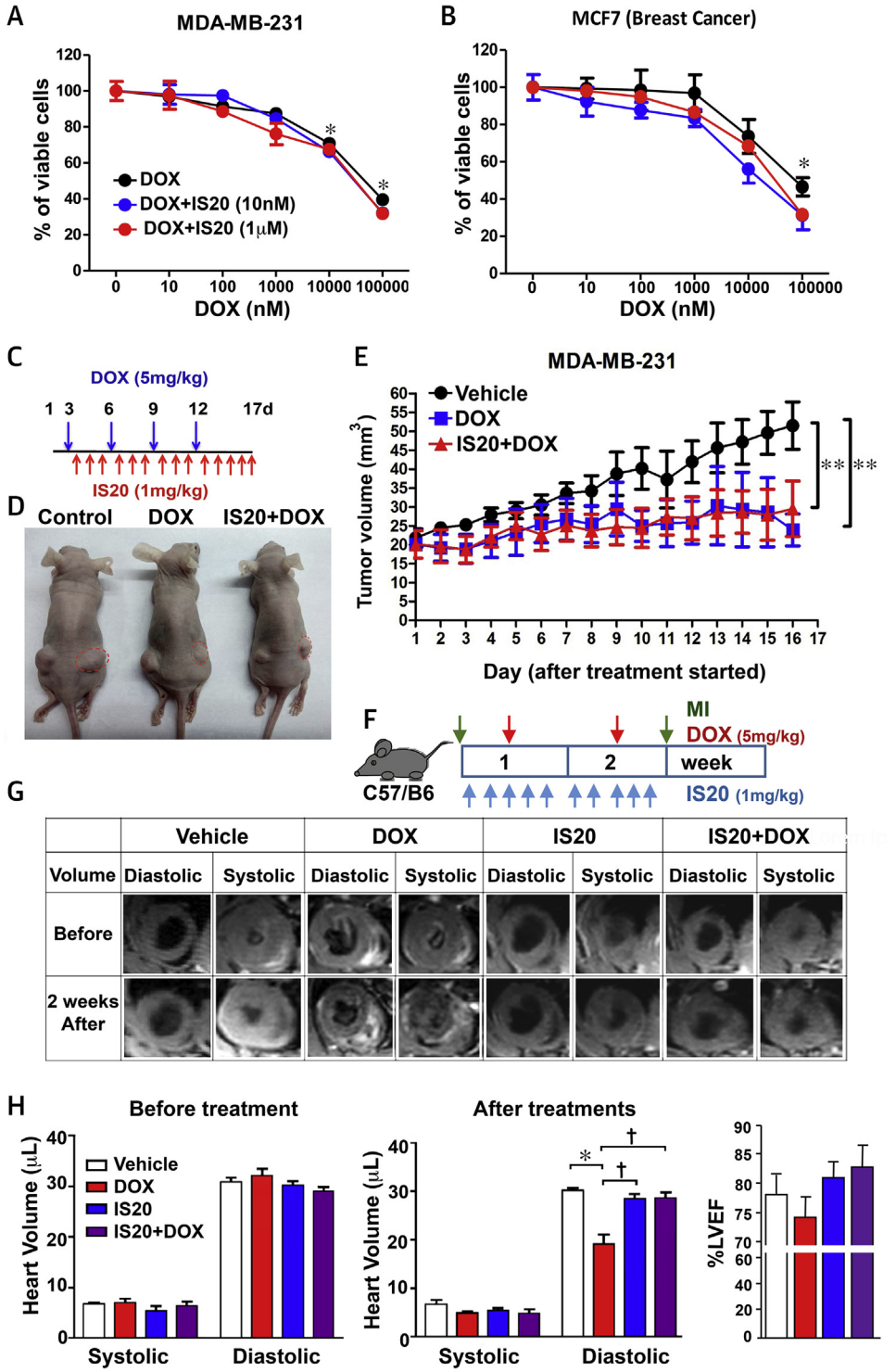

Continued on the next page

DISCUSSION

The incidence of HF during and following cancer treatment remains extremely high due to the complex molecular and pathophysiological mechanisms of cardiotoxicity and the absence of targeted cardioprotective therapeutics. We unraveled dose- and time-dependent molecular and cellular signatures of anthracycline-mediated cardiotoxicity using cardiac cells in vitro and mouse models of acute and chronic toxicity and breast cancer (**Central Illustration**). We presented evidence for a new cardioprotective strategy to mitigate cardiovascular toxicity without altering the antitumor effect of DOX via targeting PKR1 signaling.

Our data clearly demonstrated that vascular cells and resident progenitor cells in the heart were more susceptible to DOX than cardiomyocytes. We found that maximum ROS production was detected in cardiomyocytes on exposure to high concentrations of DOX (15 μM) within 3 h. However, at this setting, we found that 75 ± 8% of both ECs and hEPDCs were detached from culture dishes, indicating a detrimental effect of DOX on cell viability. We presented evidence that DOX damaged the detoxification system in cardiomyocytes by stabilizing NRF2 in the cytoplasm. NRF2 regulates antioxidant and cytoprotective gene expression in the nucleus (24). IS20 suppressed NRF2 accumulation in the cytoplasm by increasing its translocation to the nucleus. In our in vivo chronic DOX toxicity model, reduced expression of NRF2 was evident in the DOX-only treated hearts and was normalized by IS20 cotreatments. Importantly, our data demonstrated that IS20 was not a ROS scavenger and that it used the PKR1 receptor to inhibit ROS production.

The cardiotoxic effects of DOX on H9c2 and primary neonatal cardiomyocytes were attributed to the induction of apoptosis (18). We showed that prolonged medium-dose DOX promoted apoptosis not only in cardiomyocytes, but also in ECs and EDPCs. In accord with our in vitro findings, we found that activation of PKR1 by IS20 reduced H2AX phosphorylation in the long-term DOX-treated mouse hearts. AKT has been shown to preserve mitochondrial integrity and function in the heart by increasing antiapoptotic BCLl2 levels (25). Accordingly, IS20 increased the expression ratio of *Bcl2/Bax* via activation of the AKT signaling pathway because the phosphoinositide 3-kinase/AKT inhibitor reversed the antiapoptotic effect of IS20 in cardiomyocytes and EDPCs. However, IS20 activated the MAPK cascade in ECs to exert its protective effect against DOX-induced apoptosis. These data were in agreement with previous work that demonstrated that PROK2, via the PKR1 signaling, activated AKT to protect cardiomyocytes and EDPCs (26), whereas it activated MAPK to protect ECs (20).

We also observed reduced apoptosis, fibrosis, and pathological remodeling gene expression in the IS20- + DOX-treated mouse hearts. Severe fibrosis and apoptosis are hallmarks of the pathology of myocardium in patients with cumulative anthracycline therapy (23). It seemed that most of fibrosis in our chronic mouse model was replacement fibrosis, because we observed both apoptosis and fibrosis in myocardium of DOX-treated hearts.

We demonstrated that IS20 mitigated the detrimental effects of DOX that were also intrinsic to ECs and EDPCs in vitro. In HAECs, we also demonstrated that inhibition of tube formation by low-dose DOX did not induce apoptosis but increased the level of the endothelial dysfunction, indicating that endothelial dysfunction was not caused by apoptosis. In our in vivo chronic toxicity mouse model, DOX promoted vascular instability (detached ECs). In accord with previous studies (26), the capillary and vascular networks were also severely affected in DOX-treated mouse hearts. Activation of PKR1 signaling provided significant protection of vascular morphogenetic processes from DOX, leading to the establishment of interendothelial contacts and integration of ECs into the vascular wall. Hence, the increased vascular stability induced by IS20 might also contribute to the increased capillary and vessel numbers in mouse hearts cotreated with DOX.

Recently, restoration and remodeling of vascularization in tumors by angiogenic factors were shown to greatly improve intra-tumoral delivery of chemotherapeutic agents (27). For example, angiogenic

FIGURE 7 Continued

(A) Cell viability assays on MDA-MB-231 and **(B)** MCF7 breast cancer cell lines treated with different concentrations of DOX (10 to 100 μM) in the presence or absence of IS20 (10 nM or 1 μM), vehicle (zero treatment), n = 4. **(C)** Illustration of treatments 3 days after xenotransplantation of MDA-MB-231 cells. **(D)** Images of tumor size **(red dots)** on nude mice after the indicated treatments. **(E)** Quantification of tumor volumes during treatment in each group, n = 20. Data are expressed as mean ± SD. **(F)** Illustration of the acute cardiotoxicity protocol in mice (C57/B6). **(G)** Quantitative cardiac magnetic resonance analyses of heart volume during systole and diastole before treatments and 2 weeks after treatments **(left and middle)** and left ventricular ejection fraction (LVEF) **(right)**, n = 6. Abbreviations as in **Figure 1**.

CENTRAL ILLUSTRATION **Dose- and Time-Dependent Doxorubicin-Induced Cardiovascular Toxicity Is Inhibited by a GPCR Prokineticin Receptor-1 Signaling**

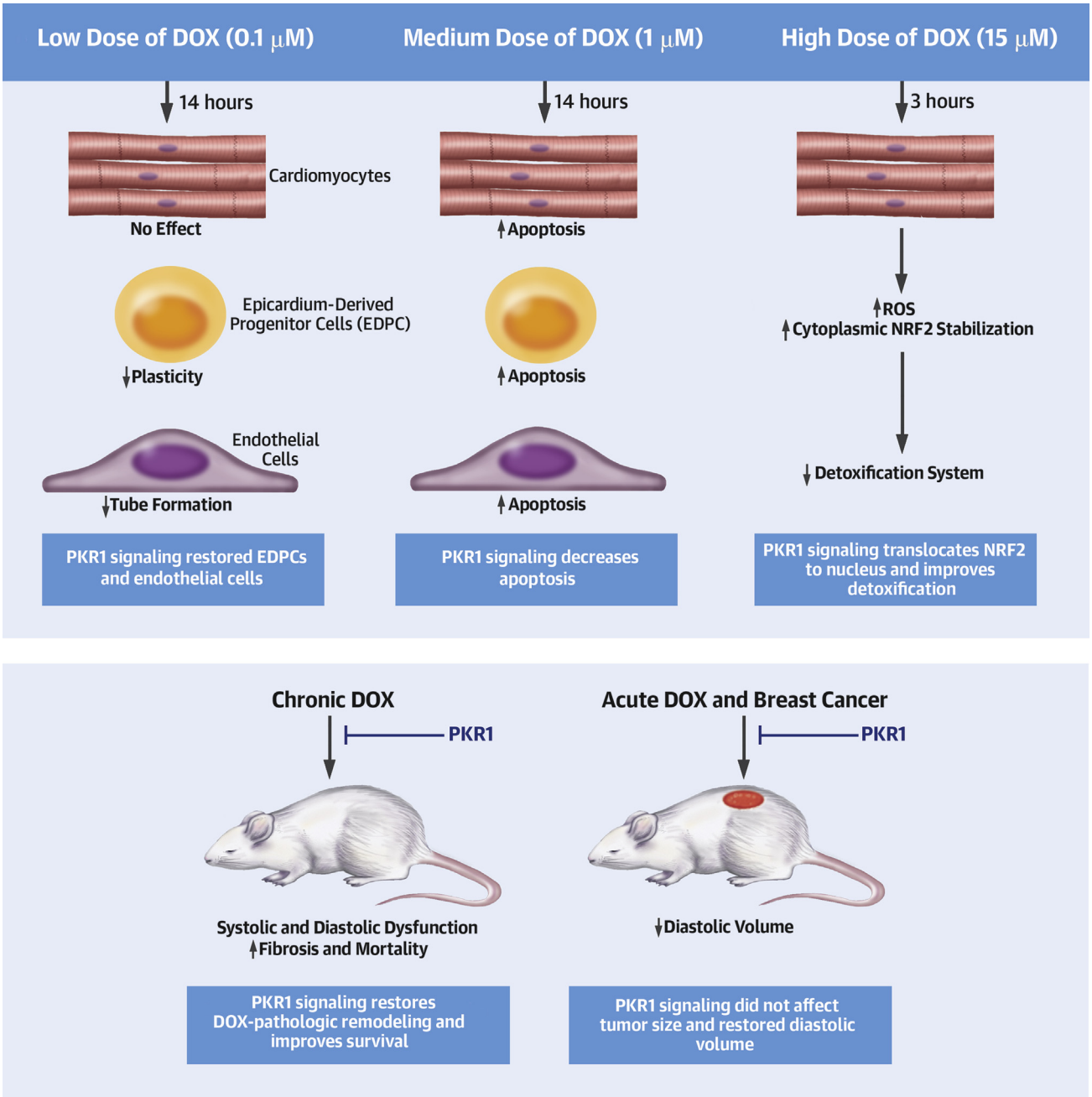

Gasser, A. et al. J Am Coll Cardiol. 2019;1(1):84–102.

We unraveled dose- and time-dependent molecular and cellular signatures of an anthracycline-mediated cardiotoxicity. Doxorubicin (DOX) at low dose **(top left)** has no effect on apoptosis or reactive oxygen species (ROS) accumulation in cardiomyocytes, whereas it reduces epicardium-derived progenitor cell (EDPC) plasticity and endothelial cell tube formation (in vitro angiogenesis). A medium dose of DOX **(top middle)** promotes apoptosis in all cardiac cells. However, a brief exposure of cardiomyocytes to a high dose of DOX **(top right)** inhibits the detoxification system via stabilizing nuclear factor erythroid-derived 2-like 2 (NRF2) in the cytoplasm, resulting in ROS accumulation. Chronic DOX cardiotoxicity in mice **(bottom left)** induces mortality with heart failure with reduced ejection fraction (HFrEF), diastolic dysfunction, and adverse cardiac remodeling, whereas acute DOX cardiotoxicity **(bottom right)** promotes diastolic volume declines. Prokineticin receptor 1 (PKR1) activation by a ligand (IS20) mitigates these detrimental effects of DOX in vitro and in vivo without altering its antitumoral effect.

factor vascular endothelial growth factor B (*Vegfb*) gene therapy inhibited DOX-induced cardiac atrophy, protected ECs from apoptosis, and preserved the myocardial capillary network (26). Although the risks associated with PKR1 activation were minimal, we also studied the effects of IS20 using in vivo tumor mouse models to check whether IS20 sensitized the tumors to DOX. IS20 did not show any mitogenic effect on cancer cells by itself and did not interfere with DOX-mediated inhibition of cell death in the cancer cells. The effects of PKR1 agonists on the normalization of vessels (20) and on extracellular matrix remodeling (12) might even be beneficial in desmoplastic tumors (e.g., breast tumors) with dysfunctional and compressed blood vessels (28).

DOX treatment was shown to permanently alter the number of stem cells in hearts (29,30). In concert with this finding, we also demonstrated that long-term exposure to DOX in mice affected the plasticity of EDPCs. In addition, we showed in vitro that low-dose DOX did not promote apoptosis, but it did diminish the number of hEPDCs. This effect of DOX was reversed by activation of PKR1 with IS20. We previously showed that in hEPDCs, PKR1 signaling via AKT activated histone demethylase KDM6A, which induced asymmetric division, leading to self-renewal and formation of vascular and epithelial/endothelial precursors (31). PKR1 signaling was shown to control EDPCs (e.g., wild-type 1^+, transcription factor 21^+ cells) formation, survival, and differentiation during embryogenesis (12) and in adult hearts exposed to metabolic changes (32). In our chronic cardiotoxicity mouse model, the recovery of heart structure and function by IS20 treatments could be partially due to recuperation of hEPDC counts, leading to repair processes in DOX-treated mice.

The pathogenesis and signaling associated with chronic DOX cardiomyopathy seem to be distinct from acute DOX cardiotoxicity. We found that DOX did not reduce the EF in acute cardiotoxicity but DOX did result in diastolic volume declines in acute mouse models. IS20 significantly alleviated DOX-induced decreases in LV diastolic volume that might occur secondary to LV remodeling in the acute toxicity mouse models. Accordingly, recent studies showed that an increase in serum troponin I might occur before EF declines in cancer patients treated with chemotherapeutics (33). Clinical studies also showed that left ventricular volumes predict adverse cardiac outcomes more reliably than EF (34,35). The evaluation of the heart volume and mass by cardiac magnetic resonance in cancer patients was recommended for the management of the risk of the HF at the early stages (33).

Several studies showed that DOX-associated cardiac morbidity and mortality in humans was associated HF with reduced EF (HFrEF) (36). In accordance with this finding, in a 2-interval DOX-mediated chronic toxicity mouse model, we observed severe mortality associated with reduced EF (HFrEF) and FS, accompanied with an elevated troponin I levels. Mice pre-treated with IS20 had a significant recovery of troponin I levels and remarkably enhanced FS and EF percentages, which resulted in an improved survival rate. Surprisingly, the systemic toxic effects of DOX, such as loss of body weight, were not completely inhibited by IS20 in vivo, despite the improvements in cardiac function and survival rate. These data eliminated the possibility that the DOX-induced mortality in our model might be caused by severe anorexia and poor oral intake. The PKR1 agonist IS20 improved heart function and the survival rate in in vivo cardiotoxicity models, counteracting DOX-mediated deficiencies in the vascular and repair systems, as well as apoptosis-mediated fibrosis and ROS production in the heart.

STUDY LIMITATIONS. A limitation of our study was the use of a concentration and/or dose of DOX, both in vitro and in vivo, that could be considered a high level. However, several studies demonstrated that DOX, at a cumulative dosage (500 mg/m^2 body surface area), led to increased ROS production in human hearts (18). Likewise, we showed that only a high concentration (15 μM) of DOX induced ROS accumulation in vitro in rodent cardiomyocytes. It was shown that the mice that received 6 mg/kg DOX (intraperitoneally) per week for 2 weeks had approximately 40 nM serum levels of DOX (26), which was in the range of serum levels (11 nm to 2 μM) observed in cancer patients who received 10 to 60 mg/m^2 of DOX (37) without mortality. We did not observe any mortality but did observe decreased diastolic volume in the acute mouse models (5 mg/kg/week for 2 weeks). However, we observed approximately 40% reduced mouse survival in our chronic cardiotoxicity model (HFrEF) with the same dose of DOX (5 mg/kg/week for 7 weeks), which could be due to accumulation of DOX in mouse cardiac tissues. Human studies also showed that DOX was not completely cleared from cardiac tissues (38), and each new administration generated an anthracycline pool that accumulated in the heart (39). Whether the serum concentration of DOX represents cardiac accumulation of DOX and whether the rodent anthracycline cardiotoxicity model is entirely representative of the causes of human HF are debatable (38). Nevertheless, our cell and animal data demonstrated that IS20 promoted

cardioprotection through PKR1 and reduced mortality induced by DOX.

CONCLUSIONS

Our data demonstrated that extensive structural damage to cardiomyocytes occurred with cumulative, increased DOX exposure; however, functional defects in the vascular system and cardiac progenitor cells might exist in response to even small doses of DOX. Moreover, we observed decreases in diastolic volume in the acute HF and HFrEF in the chronic DOX cardiotoxicity mouse models. Our in vitro and in vivo studies with genetic and pharmacological approaches demonstrated that the PKR1 specific agonist IS20 alleviated the adverse effects of DOX in cardiac cells. More importantly, IS20 did not alter the cytotoxic and antitumor effects of DOX in breast cancer lines or in mouse breast cancer models. Therefore, these data pave the way to the development of PKR1 agonists to prevent cardiovascular complications in cancer.

ACKNOWLEDGMENTS The authors thank Wan-Hong Huang (Department of Biomedical Sciences, National Chung Cheng University, Chiayi, Taiwan) and Professor Dennis W. Hwang (Institute of Biomedical Sciences, Academia Sinica, Taipei, Taiwan) for their kind assistance and thought-provoking discussions.

ADDRESS FOR CORRESPONDENCE: Dr. Canan G. Nebigil, Laboratory of Cardio-Oncology and Medicinal Chemistry, CNRS, FRE2033, Ecole Supérieure de Biotechnologie de Strasbourg, 300 Boulevard Sebastien Brant, CS 10413, F67412 Illkirch, France. E-mail: nebigil@unistra.fr. Twitter: @ECAMStrasbourg.

PERSPECTIVES

COMPETENCY IN MEDICAL KNOWLEDGE 1: Cardiotoxicity secondary to DOX is a significant adverse consequence of a highly effective chemotherapeutic agent. The mechanisms of dose- and time-dependent DOX-mediated cardiac cellular and molecular damage are unclear. Moreover, new therapeutic strategies are needed to manage the adverse cardiovascular effects of anthracyclines. We determined that vascular cells and resident progenitor cells in the heart were more susceptible to DOX than cardiomyocytes.

COMPETENCY IN MEDICAL KNOWLEDGE 2: We also suggest new cardioprotection strategies. G-protein coupled receptors play a crucial role in the regulation of cardiovascular function in both health and disease and are direct targets of more than one-third of the currently approved cardiovascular drugs used in the clinic (i.e., beta-adrenergic and angiotensin-receptor blockers). Elucidation of the roles of new cardiac G-protein coupled receptors provides targets to develop new drugs for treatment of cardiovascular diseases. Our findings reinforced previous in vitro and in vivo data that demonstrated cardioprotection through PKR1 and suggested that PKR1 agonists might be used to treat DOX cardiotoxicity and HF.

TRANSLATIONAL OUTLOOK: We examined the efficacy of IS20 in models of acute and chronic DOX cardiotoxicity. Our findings validated the cardioprotective potential of PKR1 agonists. Based on these data, next steps include the synthesis and safety, tolerability, and efficacy testing of promising IS20 derivatives as potential new candidate therapies to mitigate cardiotoxicity.

REFERENCES

1. McGowan JV, Chung R, Maulik A, Piotrowska I, Walker JM, Yellon DM. Anthracycline chemotherapy and cardiotoxicity. Cardiovasc Drugs Ther 2017;31:63–75.

2. Mertens AC, Yong J, Dietz AC, et al. Conditional survival in pediatric malignancies: analysis of data from the Childhood Cancer Survivor Study and the Surveillance, Epidemiology, and End Results Program. Cancer 2015;121:1108–17.

3. van Dalen EC, van der Pal HJ, Caron HN, Kremer LC. Different dosage schedules for reducing cardiotoxicity in cancer patients receiving anthracycline chemotherapy. Cochrane Database Syst Rev 2006:CD005008.

4. Pugazhendhi A, Edison T, Velmurugan BK, Jacob JA, Karuppusamy I. Toxicity of doxorubicin (Dox) to different experimental organ systems. Life Sci 2018;200:26–30.

5. Wang SW, Konorev EA, Kotamraju S, Joseph J, Kalivendi S, Kalyanaraman B. Doxorubicin induces apoptosis in normal and tumor cells via distinctly different mechanisms - intermediacy of H_2O_2- and p53-dependent pathways. J Biol Chem 2004;279:25535–43.

6. Zhang J, Cui X, Yan Y, et al. Research progress of cardioprotective agents for prevention of anthracycline cardiotoxicity. Am J Transl Res 2016;8:2862–75.

7. Nebigil CG. Prokineticin receptors in cardiovascular function: foe or friend? Trends Cardiovasc Med 2009;19:55–60.

8. Choke E, Cockerill GW, Laing K, et al. Whole genome-expression profiling reveals a role for immune and inflammatory response in abdominal aortic aneurysm rupture. Eur J Vasc Endovasc Surg 2009;37:305–10.

9. Urayama K, Guilini C, Messaddeq N, et al. The prokineticin receptor-1 (GPR73) promotes cardiomyocyte survival and angiogenesis. FASEB J 2007;21:2980–93.

10. Nguyen TL, Gasser A, Nebigil CG. Role of prokineticin receptor-1 in epicardial progenitor cells. J Dev Biol 2013;1:20–31.

11. Szatkowski C, Vallet J, Dormishian M, et al. Prokineticin receptor 1 as a novel suppressor of preadipocyte proliferation and differentiation to control obesity. PLoS One 2013;8:e81175.

12. Arora H, Boulberdaa M, Qureshi R, et al. Prokineticin receptor-1 signaling promotes epicardial to mesenchymal transition during heart development. Sci Rep 2016;6:25541.

13. Urayama K, Dedeoglu DB, Guilini C, et al. Transgenic myocardial overexpression of prokineticin receptor-2 (GPR73b) induces hypertrophy

and capillary vessel leakage. Cardiovasc Res 2009; 81:28–37.

14. Gasser A, Brogi S, Urayama K, et al. Discovery and cardioprotective effects of the first non-peptide agonists of the G protein-coupled prokineticin receptor-1. PLoS One 2015;10:e0121027.

15. Bernard Y, Ribeiro N, Thuaud F, et al. Flavaglines alleviate doxorubicin cardiotoxicity: implication of Hsp27. PLoS One 2011;6:e25302.

16. Congiu C, Onnis V, Deplano A, et al. A new convenient synthetic method and preliminary pharmacological characterization of triazinediones as prokineticin receptor antagonists. Eur J Med Chem 2014;81:334–40.

17. Firsanov DV, Solovjeva LV, Svetlova MP. H2AX phosphorylation at the sites of DNA double-strand breaks in cultivated mammalian cells and tissues. Clin Epigenetics 2011;2:283–97.

18. Schlitt A, Jordan K, Vordermark D, Schwamborn J, Langer T, Thomssen C. Cardiotoxicity and oncological treatments. Dtsch Arztebl Int 2014;111:161–8.

19. Li S, Wang W, Niu T, et al. Nrf2 deficiency exaggerates doxorubicin-induced cardiotoxicity and cardiac dysfunction. Oxid Med Cell Longev 2014;2014:748524.

20. Guilini C, Urayama K, Turkeri G, et al. Divergent roles of prokineticin receptors in the endothelial cells: angiogenesis and fenestration. Am J Physiol Heart Circ Physiol 2010;298: H844–52.

21. Hu G, Tang J, Zhang B, et al. A novel endothelial-specific heat shock protein HspA12B is required in both zebrafish development and endothelial functions in vitro. J Cell Sci 2006;119: 4117–26.

22. Jay SM, Murthy AC, Hawkins JF, et al. An engineered bivalent neuregulin protects against doxorubicin-induced cardiotoxicity with reduced proneoplastic potential. Circulation 2013;128: 152–61.

23. Bernaba BN, Chan JB, Lai CK, Fishbein MC. Pathology of late-onset anthracycline cardiomyopathy. Cardiovasc Pathol 2010;19:308–11.

24. Li J, Ichikawa T, Villacorta L, et al. Nrf2 protects against maladaptive cardiac responses to hemodynamic stress. Arterioscler Thromb Vasc Biol 2009;29:1843–50.

25. Gustafsson AB, Gottlieb RA. Heart mitochondria: gates of life and death. Cardiovasc Res 2008; 77:334–43.

26. Räsänen M, Degerman J, Nissinen TA, et al. VEGF-B gene therapy inhibits doxorubicin-induced cardiotoxicity by endothelial protection. Proc Natl Acad Sci U S A 2016;113:13144–9.

27. Potiron VA, Abderrahmani R, Clément-Colmou K, et al. Improved functionality of the vasculature during conventionally fractionated radiation therapy of prostate cancer. PLoS One 2013;8:e84076.

28. Gkretsi V, Stylianou A, Papageorgis P, Polydorou C, Stylianopoulos T. Remodeling components of the tumor microenvironment to enhance cancer therapy. Front Oncol 2015;5: 214.

29. Cappetta D, Rossi F, Piegari E, et al. Doxorubicin targets multiple players: a new view of an old problem. Pharmacol Res 2018;127:4–14.

30. De Angelis A, Piegari E, Cappetta D, et al. Anthracycline cardiomyopathy is mediated by depletion of the cardiac stem cell pool and is rescued by restoration of progenitor cell function. Circulation 2010;121:276–92.

31. Qureshi R, Kindo M, Boulberdaa M, von Hunolstein JJ, Steenman M, Nebigil CG. A prokineticin-driven epigenetic switch regulates human epicardial cell stemness and fate. Stem Cells 2018;36:1589–602.

32. Qureshi R, Kindo M, Arora H, Boulberdaa M, Steenman M, Nebigil CG. Prokineticin receptor-1-dependent paracrine and autocrine pathways control cardiac tcf21(+) fibroblast progenitor cell transformation into adipocytes and vascular cells. Sci Rep 2017;7:12804.

33. Han X, Zhou Y, Liu W. Precision cardio-oncology: understanding the cardiotoxicity of cancer therapy. NPJ Precis Oncol 2017;1:31.

34. Mann DL, Bogaev R, Buckberg GD. Cardiac remodelling and myocardial recovery: lost in translation? Eur J Heart Fail 2010;12:789–96.

35. Meléndez GC, Sukpraphrute B, D'Agostino RB Jr., et al. Frequency of left ventricular end-diastolic volume-mediated declines in ejection fraction in patients receiving potentially cardiotoxic cancer treatment. Am J Cardiol 2017; 119:1637–42.

36. Cardinale D, Colombo A, Bacchiani G, et al. Early detection of anthracycline cardiotoxicity and improvement with heart failure therapy. Circulation 2015;131:1981–8.

37. Liu J, Zheng H, Tang M, Ryu YC, Wang X. A therapeutic dose of doxorubicin activates ubiquitin-proteasome system-mediated proteolysis by acting on both the ubiquitination apparatus and proteasome. Am J Physiol Heart Circ Physiol 2008;295:H2541–50.

38. Salvatorelli E, Menna P, Chello M, Covino E, Minotti G. Modeling human myocardium exposure to doxorubicin defines the risk of heart failure from low-dose doxorubicin. J Pharmacol Exp Ther 2017;362:263–70.

39. Minotti G, Salvatorelli E, Menna P. Pharmacological foundations of cardio-oncology. J Pharmacol Exp Ther 2010;334:2–8.

KEY WORDS breast cancer, doxorubicin, endothelial dysfunction, epicardial progenitor cells, heart failure

APPENDIX For an expanded Methods section as well as a supplemental table and figures, please see the online version of this paper.